

# Growth Rates and Structures of MHD Modes in Stellarator/Heliotron

NAKAJIMA Noriyoshi, NÜHRENBERG Carolin<sup>1</sup> and NÜHRENBERG Jürgen<sup>1</sup>

*National Institute for Fusion Science, Toki, 509-5292, Japan*

*<sup>1</sup>Max-Planck-Institut für Plasmaphysik, D-17491 Greifswald, Germany*

(Received: 21 January 2004 / Accepted: 11 March 2004)

## Abstract

Recently, high- $\beta$  plasmas with  $\langle\beta\rangle \sim 3\%$  have been established in two different types of helical devices, namely, Large Helical Device (LHD) and Wendelstein 7-AS (W7-AS). These devices are designed with complementary physics concepts. The purpose of the present work is to theoretically understand the properties of ideal Magneto-Hydro-Dynamics (MHD) instabilities in those high- $\beta$  plasmas and to try to explain the experimental results on a common theoretical basis, namely, the linearized ideal MHD global mode analyses using compressible perturbations. Physically correct growth rates and mode structures make the direct comparison between theory and experiment possible.

## Keywords:

ideal MHD, growth rate, stellarator, heliotron

## 1. Introduction

In order to investigate the ideal MHD stability in stellarator/heliotron, linearized ideal MHD stability analyses have been performed by assuming that the perturbations or displacement vectors  $\xi$  in the energy principle form are incompressible, since the stability criterion of pressure-driven modes with resonant rational surfaces, determined only by the sign of the potential energy, does not change whether the perturbations are incompressible or not. Moreover, such incompressible analyses have been performed under the fixed boundary condition, namely the condition that the normal displacement  $\xi^s$  is not allowed on the plasma-vacuum boundary. These incompressible analyses under the fixed boundary condition are not so time consuming that they are suitable to the fast analyses of the reconstructed MHD equilibria from the experimental data or analyses based on the theoretically prepared MHD equilibrium data base. In those incompressible stability analyses, however, the growth rates do not have correct physical meaning and the profiles of eigenfunctions are not exact, because the component of the displacement vector parallel to the equilibrium magnetic field  $\xi^{\parallel}$  is not included, or more physically, the branch of the slow magnetosonic is not included. Therefore, in order to compare between theoretical and experimental results, to be done firstly from the theoretical point of view is to perform the MHD stability analyses avoiding a possible discrepancy between theoretical and experimental results. For such a purpose, here, ideal compressible MHD analyses are performed under the free boundary

condition, so that physical growth rates and eigenfunctions can be correctly evaluated.

Recently, high- $\beta$  plasmas with  $\langle\beta\rangle \sim 3\%$  have been established in two different types of helical devices, namely, LHD [1] and W7-AS [2]. These devices are designed with complementary physics concepts as to make two main different lines in researches of the three dimensional configurations. In the case of LHD, high  $\beta$  plasmas are established in the inward-shifted configurations with the vacuum magnetic axis  $R_{ax}$  of 3.6 m, where pressure-driven modes are theoretically more unstable compared with those in the standard configuration with  $R_{ax} = 3.75$  m or in the outward-shifted configurations with  $R_{ax} \sim 3.9$  m, when the MHD equilibria with same pressure and current conditions are used by only changing the plasma boundary shape. At present, the typical high- $\beta$  MHD equilibria in the inward-shifted configurations are not rigorously fixed from the experimental point of view, thus, theoretically chosen MHD equilibria are used in this work.

The second line of stellarators is represented by W7-AS and by W7-X. In W7-AS, the maximum  $\beta$  was obtained with  $B = 0.9$  T,  $\langle\beta\rangle \sim 3.2\%$  with a flat top time of  $\sim 0.35$  s. Above  $\langle\beta\rangle \sim 2.4\%$  the Mirnov diagnostic shows the discharge to be quiescent. In the computational reconstruction of such a discharge (#51755), the rotational transform was found to vary substantially. In keeping with the experimental measurements, the low-node-number global ideal MHD modes (dominantly  $n = 1$ ) have computationally been found unstable up to  $\langle\beta\rangle \sim$

2.4 %. Computationally obtained, maximum physical, growth rate is 14 kHz. Because interchange stability prevails in W7-X, the present work clarifies the role of local ballooning stability  $\beta$  limit.

## 2. Properties of pressure-driven modes in inward-shifted LHD configurations

To understand the overall properties of pressure-driven modes in inward-shifted LHD configurations, three MHD equilibria with  $\langle\beta\rangle = 1\%$ ,  $2\%$  and  $3\%$  are created under both fixed boundary and currentless conditions by using VMEC code [3], where 300 radial meshes, and 7 poloidal and 12 toroidal Fourier modes are used, respectively. The used plasma boundary is so small that the plasma volume is around  $25\text{ m}^3$  and the rotational transform at the plasma boundary is around 1.36. The used pressure profile is  $P(s) = P(0)(1-s)(1-s^9)$ , where  $s$  is the normalized toroidal flux, which is related to the normalized minor radius  $\rho$  as  $\rho = \sqrt{s}$ . The rotational transform  $\iota$  and Mercier index  $D_I$  for  $\langle\beta\rangle = 1\%$ ,  $2\%$  and  $3\%$  are shown in Fig. 1. The  $\iota$  almost monotonically increases in any cases, and all equilibria are Mercier-unstable except for plasma periphery. The MHD equilibria are calculated under the fixed boundary condition, so that the stabilizing effects by the free boundary motion of the plasma boundary are reduced, leading to the increase of  $D_I$  as  $\beta$  increases. Note that it is considered that the theoretically chosen MHD equilibria, used here, are more unstable than experimentally observed ones.

The ideal MHD stability analyses for compressible perturbations are performed by the cas3d3 code [4], where 300 radial meshes, 20 poloidal and 20 toroidal Fourier modes in the Boozer coordinates are used for the mapping of equilibrium. As a perturbation, 60 Fourier modes are used to express each component in  $\xi_{\perp}^{\parallel}$ , the component perpendicular to the equilibrium magnetic field, and 490 Fourier modes are used for  $\xi^{\parallel}$ . Note that quite large Fourier space is needed to correctly express the incompressible properties of the perturbations in the compressible calculations [4]. The radial width of the most unstable mode for each toroidal mode number  $n$  is shown in Fig. 2, where the radial width is roughly defined as the region that the amplitude of the eigenfunction is larger than 70 % of the peak value. The radial width for the free (fixed) boundary condition is indicated by the solid (dotted) lines.

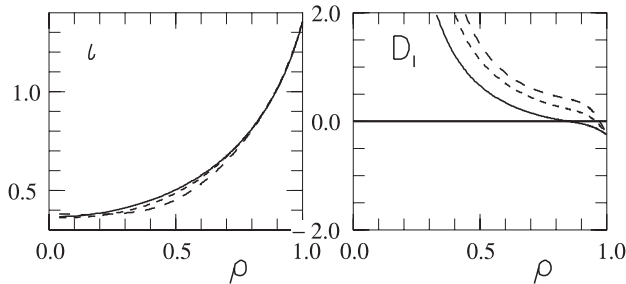


Fig. 1 Radial profiles of  $\iota$  and  $D_I$  in inward-shifted LHD plasmas. The solid, short dotted, and long dotted lines correspond to  $\langle\beta\rangle = 1\%$ ,  $2\%$ , and  $3\%$  respectively.

(dotted) lines, with the location of the dominant modes shown by open rectangles (free boundary) and open circles (fixed boundary), and the location of the dominant low- $m$  rational surfaces, namely  $\iota = 0.4, 0.5, 0.6, 0.75$  and  $1.0$ . Since the MHD equilibria are Mercier unstable, the toroidal mode coupling inherent to helical systems is so weak [5,6] that the toroidal mode number  $n$  can be used as a good quantum number. Therefore, to distinguish the unstable eigenvalues by the radial node number is also possible for both interchange modes consisting of multiple Fourier modes and ballooning modes. It is understood that 1) the unstable region moves from plasma core to plasma periphery as  $\beta$  increases, 2) the lower the toroidal mode number  $n$  is, the wider the radial width is, and also this tendency becomes clear in low- $\beta$  plasmas, 3) the free boundary motions become important for low- $n$  modes with a global structure under the fixed boundary condition, and/or for high- $\beta$  plasmas, and 4) the unstable radial region does not depend on the toroidal mode number  $n$  so much, leading to the simultaneous excitation of many linearly independent modes around same radial location. For more detail, see Fig. 3. The movement of the unstable region is correlated with the magnetic well formation by the Shafranov shift. When  $\langle\beta\rangle$  increases more, the Mercier stable region appears in the plasma core region. This tendency is

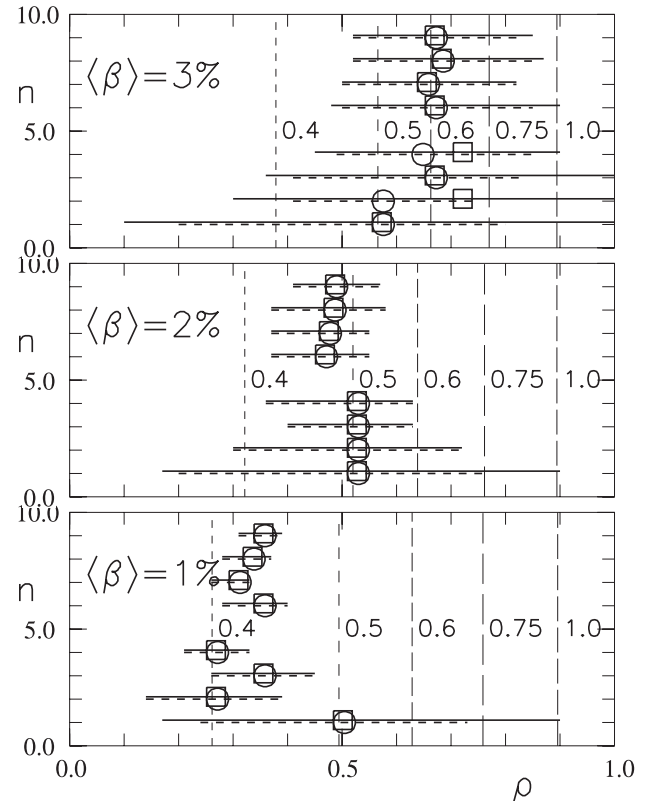


Fig. 2 Radial width of unstable modes vs toroidal mode number  $n$  in inward-shifted LHD with  $\langle\beta\rangle = 1\%$ ,  $2\%$ , and  $3\%$ . The solid (dotted) lines correspond to free (fixed) boundary condition, and Open rectangles (circles) indicate the location of the dominant Fourier modes for free (fixed) boundary condition. The location of the dominant low- $m$  rational surfaces is also shown by vertical lines with the value of  $\iota$ .

already reflected on the movement of the unstable region. In some cases, the dominant modes changes from fixed boundary condition to free boundary condition, say,  $n = 2$  and 4. Note that in these equilibria, the rational surface with  $\iota = 0.5$  always exists inside of the plasma, leading to the global modes with  $(m, n) = (2, 1)$  even for low- $\beta$  plasma, and that the dominant poloidal mode numbers are fairly large for  $n > 5$ .

Figure 3 shows the growth rate normalized by the Alfvén transit time on the magnetic axis:  $\gamma\tau_{A0}$  and the type of modes. For low- $\beta$  case ( $\langle\beta\rangle = 1\%$ ), all unstable modes are interchange modes with only single dominant Fourier mode. Except for  $(m, n) = (2, 1)$ , all modes are localized modes as is also understood from Fig. 2. As  $\beta$  increases, such interchange modes with single dominant Fourier mode change into localized interchange modes consisting of multiple Fourier components except for  $(m, n) = (2, 1)$  and  $(m, n) = (4, 2)$  for, say,  $\langle\beta\rangle = 2\%$ . And finally, almost all modes except for low- $n$  modes change into ballooning modes. There are several important features: 1) there is a case that low- $n$  global interchange modes under the fixed boundary condition change into ballooning modes under the free boundary condition as  $\beta$  in-

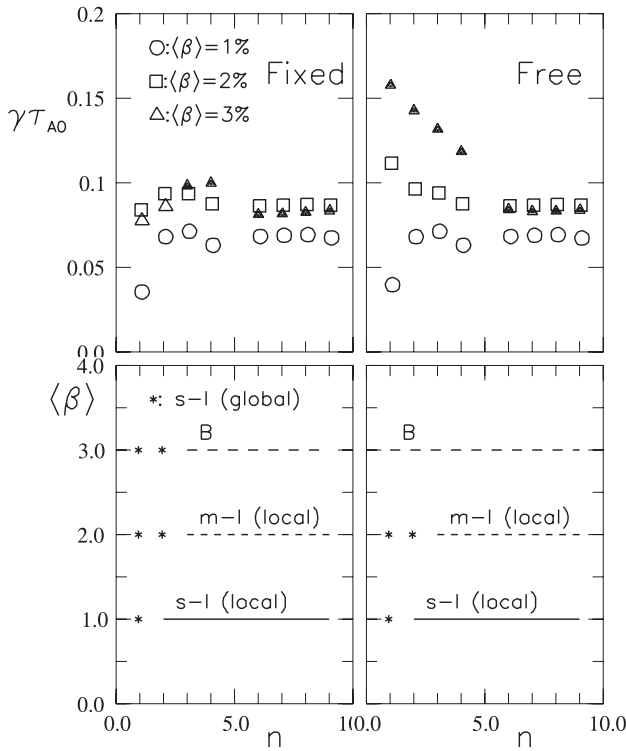


Fig. 3 Normalized growth rates and type of modes vs toroidal mode number  $n$  in inward-shifted LHD with  $\langle\beta\rangle = 1\%$ ,  $2\%$ , and  $3\%$ . The left and right columns correspond to fixed and free boundary condition, respectively. In the upper two figures, the open circles, rectangles, triangles denote interchange modes, and the solid triangles indicate ballooning modes. In the lower two figures, s-l and m-l means interchange modes consisting of single dominant Fourier mode and multiple Fourier modes, respectively, and B means a ballooning mode. Attached global (local) indicates a global (local) mode.

creases, 2) up to around  $3\%$ , the growth rates for a specified toroidal mode number do not change so much even if  $\beta$ -value changes, and for typical high- $\beta$  LHD operation parameters, the order of the growth rates is around  $40\ \mu\text{sec}$  ( $\gamma\tau_{A0} = 0.1$  corresponds to around  $40\ \mu\text{sec}$ ), 3) the growth rates do not depend on the toroidal mode number so much, and so taking account of the radial positions of the unstable modes in Fig. 2, many modes may be simultaneously excited around the same radial location, and 4) for high- $\beta$  equilibria, free boundary analyses are inevitable. As an example, the normal displacement  $\xi^s$  of  $n = 3$  mode for  $\langle\beta\rangle = 3\%$  is shown in Fig. 4 for both free and fixed boundary conditions. It is understood that when the free boundary motion of the perturbation is allowed on the plasma-vacuum boundary, the Fourier modes near the plasma periphery are excited, leading to a more global profile. Another interesting point is that the experimentally observed modes  $(m, n) = (2, 3)$  [7], whose resonant surface is outside of the plasma, is excited near the plasma periphery.

The radial distributions of the potential energy  $W_P$  and kinetic energy  $W_K$  are shown in Fig. 5 and Fig. 6, respectively, for the ballooning mode under free boundary condition in Fig. 4. The potential energy is divided into the shear Alfvén term noted by 1, the fast magnetosonic term by 2 (quite small), the slow magnetosonic term by 3 (magnified 5 times), the pressure-driven term by 4, the current-driven term by 5.  $W_P$  itself is indicated by 6. The kinetic energy is divided into two parts: one is due to  $\xi^{\parallel}$  ( $W_K(\xi^{\parallel})$ ) indicated by 1, and the other is due to  $\xi^{\perp}$  ( $W_K(\xi^{\perp})$ ) by 2.  $W_K$  itself is indicated by 3. The kinetic energy  $W_K$  of the unstable modes mainly comes from the component of the displacement vector parallel to the equilibrium magnetic field  $\xi^{\parallel}$ , namely  $W_K(\xi^{\parallel}) \geq W_K(\xi^{\perp})$ . This is due to the fact that the incompressibility condition is almost satisfied except for the mode rational surfaces as shown in Fig. 5, so that a strong  $\xi^{\parallel}$  is created around the mode rational surfaces as shown in Fig. 6. This tendency becomes stronger for interchange modes with an almost uniform amplitude of the perturbed pressure along the equilibrium magnetic field line, compared with ballooning modes where the amplitude of the perturbed pressure is non-uniform along the equilibrium magnetic field line. In the present analyses,  $W_K(\xi^{\parallel})/W_K(\xi^{\perp}) \sim 4$  for interchange modes, and  $W_K(\xi^{\parallel})/W_K(\xi^{\perp}) \geq 1$  for ballooning modes. As  $\beta$  increases or modes become more unstable,

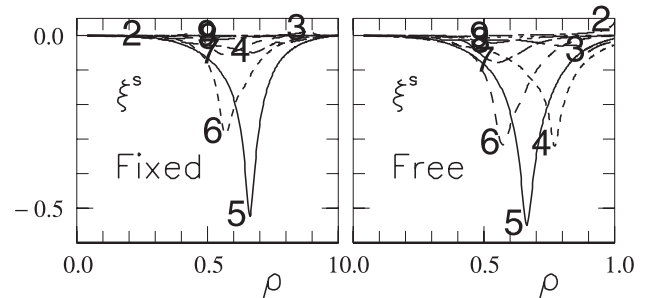


Fig. 4 Radial profile of  $\xi^s$  for  $n = 3$  under fixed (left) and free (right) boundary condition in LHD with  $\langle\beta\rangle = 3\%$ . The attached numbers indicate the poloidal mode numbers.

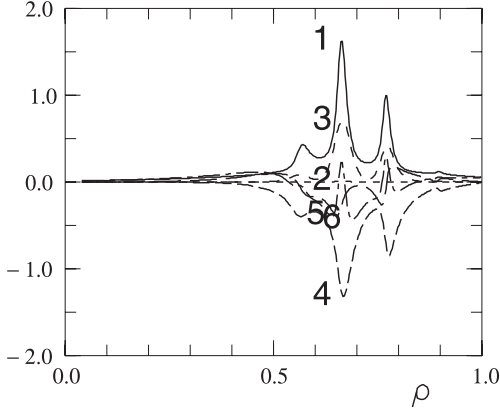


Fig. 5 Radial profile of potential energy corresponding to Fig. 4. Slow magnetosonic term denoted by 3 is magnified 5 times.

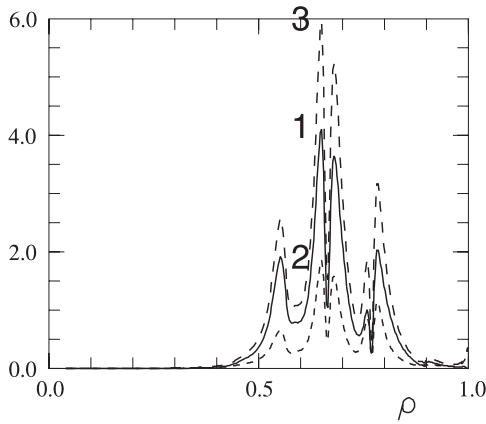


Fig. 6 Radial profile of kinetic energy corresponding to Fig. 4.

the contribution by  $\xi^{\parallel}$  becomes same as that by  $\vec{\xi}_{\perp}$ . Note that, in usual incompressible treatments,  $\xi^{\parallel}$  component is eliminated in both linear and nonlinear calculations.

In the incompressible perturbations, the counter parts of the unstable modes are shear Alfvén modes, since the slow magnetosonic waves are excluded. In contrast with it, the counter parts of the unstable modes become slow magnetosonic waves for the compressible perturbations, since the shear Alfvén continuum spectrum moves up from the marginal point [4]. These properties in the stable side of the ideal MHD spectrum will influence on the point spectra like Toroidicity-induced Alfvén Eigenmodes, and Helicity-induced Alfvén Eigenmodes in LHD configuration.

### 3. High- $\beta$ W7-AS discharge

A series of equilibria representing the W7-AS discharge #51755 has been studied for its ideal MHD properties using the CAS3D [8] global stability code. All equilibrium properties referred to below originate from the computational reconstruction (NEMEC code by S.P. Hirshman, calculation: courtesy J. Geiger) and match the experimental measurements according to the quality of the reconstruction. In the discharge W7-AS #51755  $\langle\beta\rangle \approx 3.1\%$  was achieved with  $\beta(0) \approx 7\%$  for a flat top time of  $> 0.1$  s [2]. The VMEC flux-surface

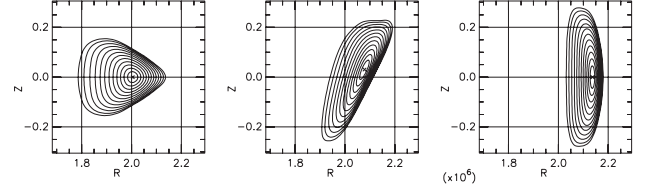


Fig. 7 Flux-surface cross-sections for the W7-AS discharge #51755 at  $\langle\beta\rangle = 3\%$  (NEMEC by S.P. Hirshman, calculation: courtesy J. Geiger).

cross-sections at  $\langle\beta\rangle \approx 3.1\%$  are shown in Fig. 7. The rotational transform  $\iota$  changes significantly with the plasma- $\beta$ : from monotonically increasing towards the plasma edge and  $\iota < 1/2$  at  $\beta(0) \approx 0$  to monotonically decreasing with  $\iota = 1/2$  inside the plasma for  $\langle\beta\rangle > 1\%$ . Also,  $\iota$  steepens with increasing  $\beta$ . In the global stability analyses (CAS3D, 101 radial grid points, 64 perturbation harmonics, free-boundary, finite adiabatic index  $5/3$ , non-uniform equilibrium mass density profile) the  $m = 2, n = 1$  perturbation harmonics mostly dominate (see Fig. 8 for normal displacements harmonics at  $\langle\beta\rangle \approx 0.84\%$ ). A  $\beta$ -scan of the growth rates is given in Fig. 9; here, the electron number density was at  $n_e(0) \approx 2.4 \times 10^{20} \text{ m}^{-3}$  at  $\langle\beta\rangle \approx 3.1\%$  (comm. by A. Weller). The growth-rate peak at  $\langle\beta\rangle \approx 2\%$  is due to the occurrence of  $\iota = 5/11$  just outside the plasma boundary. The global mode analysis finds stability beyond  $\langle\beta\rangle \approx 2.3\%$ , which is in keeping with the measurements that also see very little MHD activity beyond  $\iota = 0.24$  s or  $\langle\beta\rangle \approx 2.3\%$  [2].

### 4. Standard high-mirror W7-X

Global ballooning modes have been studied in the W7-X standard high-mirror case (see Ref. [8] for the plasma boundary and Fig. 10 for the flux-surface cross-sections at  $\langle\beta\rangle \approx 5\%$ ) in order to understand the meaning of the theoretical local ballooning limit, which is  $\langle\beta\rangle \approx 5\%$ . For the high-mirror cases,  $|B_{max} - B_{min}|/(2\bar{B}_0) \approx 0.1$  is the mirror field on the magnetic axis. With  $\beta = 0.08 \times T[\text{kV}]n[10^{20}]/B_0^2[\text{T}]$ , a number density  $n(0) = 3 \times 10^{20} \text{ m}^{-3}$ , a temperature of  $T(0) = 3$  kV, and the magnetic field  $B_0(0) = 2.5$  T correspond to  $\beta(0) = 12\%$  or  $\langle\beta\rangle = 5\%$  for the profile used. In W7-X equilibria the rotational transform typically changes only very little with increasing  $\beta$ , for the standard case  $5/6 < \iota < 5/5$ . All the equilibria studied here are locally Mercier stable. In Fig. 11, the normal-displacement harmonics are shown for an unstable perturbation at  $\langle\beta\rangle = 6.3\%$ . Stellarator-type coupling is important [ $(m = 14, n = 12)$  and  $(m = 20, n = 17)$ ]. With its many side-bands and the maximum-amplitude regions on the outside of the torus, the perturbation is manifestly ballooning-type (101 radial points, 280 mode harmonics). The  $\beta$ -scan of the growth-rates (compare Fig. 12) shows that all global stability limits are above  $\langle\beta\rangle = 5\%$ , the higher poloidal-node-number perturbations ( $m = 55$ ) being closest. With low-node-number global perturbations ( $m = 14$ ) a global stability limit of  $\langle\beta\rangle = 6\%$  is found, which is above the local ballooning limit.

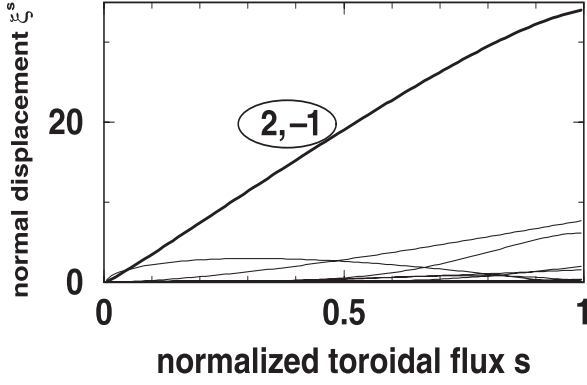


Fig. 8 CAS3D normal-displacement harmonics of an unstable essentially  $m = 2$  perturbation versus  $s$  in W7-AS #51755 at  $\langle\beta\rangle = 0.84\%$ .

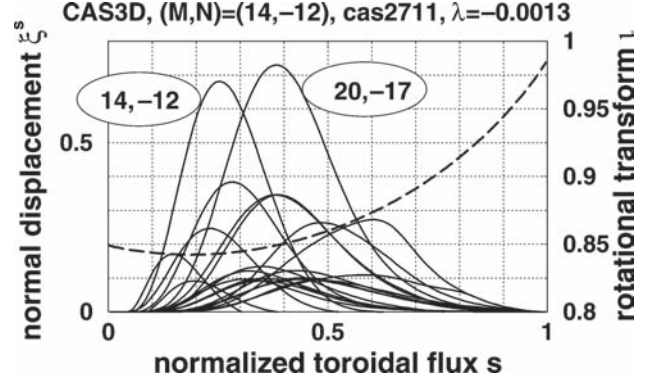


Fig. 11 CAS3D normal-displacement harmonics of an unstable low- $m$  perturbation in the standard high-mirror W7-X at  $\langle\beta\rangle = 6.3\%$ .

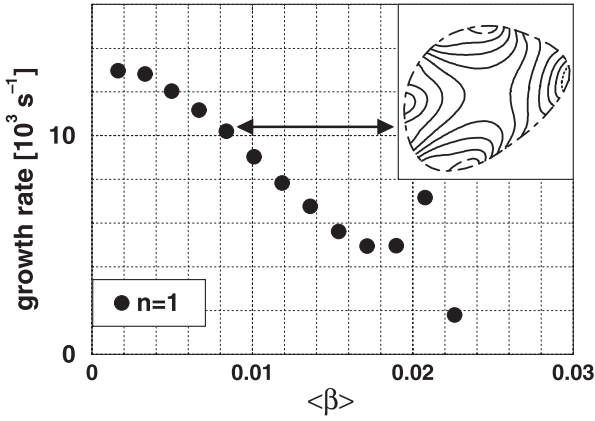


Fig. 9 Plasma- $\beta$  scan of MHD growth rates,  $\gamma$ , in W7-AS discharge #51755. The inset shows perturbed pressure contours ( $\varphi = 4^\circ$ , essentially  $m = 2$ ,  $n = 1$ ,  $\langle\beta\rangle = 0.84\%$ , compare Fig. 7).

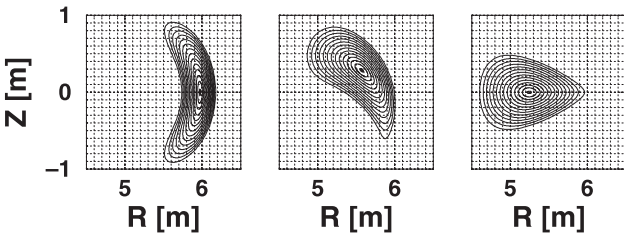


Fig. 10 Flux-surface cross-sections for the W7-X standard high-mirror case at  $\langle\beta\rangle = 5\%$  [2].

## 5. Discussions

It is thought from results on inward-shifted LHD configurations that used fixed boundary MHD equilibria are considerably more unstable than experimentally observed plasmas. Therefore, more detail analyses of ideal MHD instabilities in inward-shifted LHD configurations should be performed by using the reconstructed MHD equilibria based on the experimental data, in order to clarify whether ideal

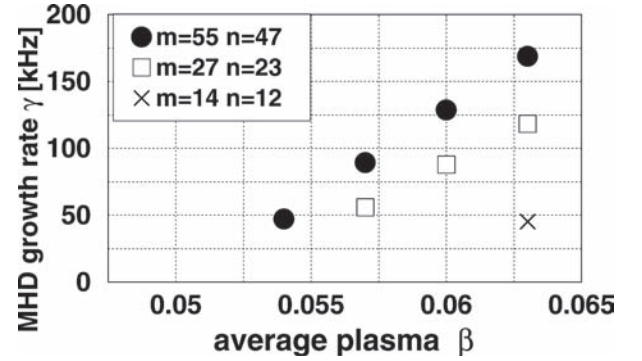


Fig. 12 Plasma- $\beta$  scan of MHD growth rates,  $\gamma$ , for the W7-X standard high-mirror case.

MHD stability theory, as it is, is useful or not. If there still were discrepancies between theory and experiment for reconstructed MHD equilibria, then we have to consider the non-ideal effects like two-fluids effects, nonlinear effects and so on. Moreover, we have to answer why ideal MHD theory is not applicable to inward-shifted LHD configurations, because there are fairly good consistency between theory and experimental results in W7-AS as shown here and tokamaks.

Related to the discrepancy, if any, the treatment of the stochastic region surrounding the plasma in the nested flux surface region is also important issue. In the case of tokamaks, there is no such a stochastic region basically, and in W7-AS the connection length in the stochastic region is so short compared with LHD that such a stochastic region is treated as vacuum region. In the case of LHD configurations, however, the connection length in the stochastic region is so long compared with parallel mean free path of particles that there is a possibility that a force free ideal or resistive plasma exists there, which leads to stabilizing effects compared with vacuum. In order to clarify above problems, comparative studies among LHD, W7-AS, W7-X and tokamaks are quite useful, which leads to deeper understanding of the ideal MHD theory in torus systems.

## References

- [1] O. Motojima *et al.*, Nucl. Fusion **43**, 1674 (2003).
- [2] A. Weller *et al.*, *Proc. 13th ISW Canberra* at <http://www.rsphysse.anu.edu.au/admin/stellarator/>
- [3] S.P. Hirshman, Phys. Fluids **26**, 3553 (1983).
- [4] C. Nührenberg, Phys. Plasmas **6**, 137 (1999).
- [5] N. Nakajima, Phys. Plasmas **3**, 4556 (1996).
- [6] J. Chen, N. Nakajima and M. Okamoto, Phys. Plasmas **6**, 1562 (1999).
- [7] S. Sakakibara *et al.*, Plasma Phys. Control. Fusion **44**, A217 (2002).
- [8] C. Nührenberg, Phys. Plasmas **3**, 2401 (1996).